Correlation of an antimicrobial peptide's potency and its influences on membrane elasticity

Wen-Fang Chang, Si-Han Chen, and Yi-Fan Chen*
Department of Chemical and Materials Engineering, National Central University, Taoyuan 32001, Taiwan

(Received 21 April 2018; revised manuscript received 9 August 2018; published 15 October 2018)

The killing power of membrane-active antimicrobial peptides (AMPs) lies in their ability to disrupt the structures of pathogenic membranes. While understanding the AMPs' mechanisms of action is key to realizing their therapeutic potentials, how the AMPs modulate membrane elasticity and thereby affect membrane structure remains an open question, even though the AMP-induced variations in membrane curvature are widely considered to be crucial. Here, we exploit the x-ray diffraction technique to examine how the dominant bacterial lipid, phosphatidylethanolamine, varies its monolayer elastic properties upon interacting with six artificial peptides mimicking the AMPs' common amino acid content. Remarkably, the monolayer spontaneous curvature C_0 is unaffected by any of the peptides. In contrast, the peptides designated as $(K2W)^2$, K4W2, R6, and R9, mimicking the AMP mutants with microbicidal potency, are able to modify the monolayer bending moduli K_{cp}, while those derived from the impotent mutants cannot. The results are consistent with the scenario that the AMPs disrupt the structure of pathogenic monolayers by, additionally if not exclusively, modulating their K_{cp}'s, with stiffening and softening leading to two different modes of disruption, that is, toroidal pore formation and membrane micellation, respectively.

DOI: 10.1103/PhysRevE.98.042408

I. INTRODUCTION

Membrane-active antimicrobial peptides (AMPs) kill pathogens by structurally disrupting their membranes. With membranes being their targets, the AMPs are less susceptible than conventional antibiotics to drug resistance and are thus considered as promising alternatives to conventional antibiotics. The structural disruption to pathogenic membranes by the AMPs may involve the formation of transmembrane pores, which dissipate vital biochemical gradients across the membranes or even lead to pathogen rupture [1–3]. Forming the pores often entails the membranes, whose bilayer structure consists of two monolayers (i.e., monomolecular layer of lipid), to convert from a planar monolayer conformation to a nonplanar one [4–7] and therefore concerns monolayer elasticity. To unleash the AMPs' full potential, researchers have been paying great attention to the mechanisms of pore formation, particularly to how the AMP influences on monolayer elasticity are dictated by the sequence of their building block, amino acids (AAs) [8–11]. Nevertheless, even with hefty investments of research efforts, the relations remain elusive.

Despite being widely diverse in many aspects, the AMPs are commonly cationic, and many are enriched in the cationic AAs, arginine (R) and lysine (K) [12]. By scrutinizing the AMP, defensin, and the mutants, Wong and colleagues suggest that membrane-active AMPs' richness in R is to facilitate formation of the nonplanar monolayer conformations which are featured with negative Gaussian curvatures G's and are the underlying conformations of transmembrane pores [9,13–15]. The researchers further indicate that the AMPs' specificity toward bacteria rather than eukaryotic host cells arises from the discrepancy in the abundance of the zwitterionic lipid, phosphatidylethanolamine (PE), in the membranes, which exhibits a great tendency to assume an inverted nonplanar monolayer conformation and thus possesses the monolayer spontaneous curvature C_0 of highly negative values [16–18]. Membranes enriched in PE (e.g., bacterial cell membranes), they claim, are more susceptible than those with reduced PE contents (e.g., eukaryotic cell membranes) to the AMP-induced structural transformations that lead to the nonplanar conformations with negative G's [9,13–15]. It was also found in their studies that substituting K for the Rs in the defensin crippled the AMP's ability to drive the planar conformation into the nonplanar ones with negative G's. Remarkably, the compromising effect of the mutation could be reversed when Ks were substituted along with hydrophobic amino acids (HAAs) [13]. (Note that when talking monolayers here and in the following, we refer NOT to a standalone monolayer formed on the air-liquid interface but to a monolayer which is the half part of a bilayer.)

In the context of the continuum mechanics model for membrane elasticity, the aforementioned observations imply that the Rs, or the Ks coupled with HAAs, in the AMPs exert substantial influences on the elastic properties of lipid monolayers. Indeed, many endeavors in understanding the AMPs' mechanisms of action have been focusing on their influences on the monolayers' tendency of assuming a nonplanar conformation and therefore on C_0 (Ref. [19] and references therein). Nevertheless, most of the conclusions regarding the AMPs' effects on C_0 were drawn from how the phase behavior, specifically, a planar-to-nonplanar phase transition temperature, of a lipid monolayer shifted under the influence of the AMPs. Few studies, if any, have ever directly measured the AMP-induced variations in C_0 such that the

*yifanchen@ncu.edu.tw

 ©2018 American Physical Society

C_0-centered view on the AMPs' mechanisms of action can be verified. Furthermore, C_0 is not the sole elastic property that dictates the phase behavior; other elastic properties, such as the bending modulus K_{cp}, which measures monolayer bending rigidity, make significant contributions, too. Direct and systematic investigations on the variations in K_{cp} in response to the AMPs' action are even rarer (prominent exceptions being Refs. [20,21]).

To explore the physical insights underlying the aforementioned observations, this paper examines how the short peptides made of R, K, or K coupled with HAA, tryptophan (W), in different lengths and orders modulate the C_0's and K_{cp}'s of the lipid monolayers comprising the PE species of dioleoylphosphatidylethanolamine (DOPE) or DOPE mixed with the anionic lipid, dioleoyl phosphatidic acid (DOPA), in the molar ratio of 96:4. The PE-majority monolayers were chosen because of PE's dominance in bacterial cell membranes (e.g., 80% of total lipids in *E. coli* [22]), while the peptides were designed so as to reflect the common AA content of the AMPs and capture the essential features of defensin and the mutants studied by Wong and colleagues. Through this study, we also aspire to uncover the physical principles underlying membrane-AMP interaction that will one day guide the design of synthetic AMPs.

II. EXPERIMENTAL

A. Materials

DOPE (cat. no. 850725C) and DOPA (cat. no. 840875C) dissolved in chloroform were purchased from Avanti (Alabaster, AL) and used without further purification. Synthetic peptides, KKKKKK, KKKKKKKKK, KKWKKW, KKKKWW, RRRRRR, and RRRRRRRRR, designated as K6, K9, $(K2W)^2$, K4W2, R6, and R9, respectively, were synthesized and purified to >95% by Kelowna International Scientific (New Taipei, Taiwan) and also used as received. $(K2W)^2$, K4W2, R6, and R9 were to mimic the microbicidal-potent AMP mutants investigated by Wong and colleagues [13], while K6 and K9 corresponded to the ones without microbicidal potency. Tetradecane (cat. no. 87140), 2-methylbutane (cat. no. M32631), and polyethylene glycol 8000 (PEG 8000; cat. no. P2139) were purchased from Sigma-Aldrich (St. Louis, MO), and phosphate buffered saline (PBS) solution (cat. no. PBS001) was purchased from Uni-Onward (New Taipei, Taiwan); all were used as received.

B. Sample preparation

Lipids dispersed in pH-buffered solutions were used for the C_0 and K_{cp} measurements and prepared following a well-established procedure [16,23]. In brief, DOPE and DOPA were mixed in a desired molar ratio, either DOPE : DOPA = 100:0 or 96:4, in chloroform, with the total dry lipid weight in 8 mg. After chloroform was evaporated with a gentle flow of argon gas, the sample was placed under vacuum overnight to remove residual chloroform. This was followed by adding tetradecane to the dried lipid film and dissolving the mixture in 2-methylbutane to well mix the two specimens. The addition of tetradecane was to relieve the packing frustration in the hydrophobic regions of the inverted hexagonal H_{II} phase such that the water core radius of the H_{II} phase was directly correlated with C_0 (see below). 2-Methylbutane was subsequently removed as in the removal of chloroform, although care was especially taken to ensure the total evaporation of 2-methylbutane before any escape of tetradecane. The dried lipid film, containing the lipids in one of the two desired molar ratios and 16 wt % tetradecane, was suspended in 100 μl of 10 mM PBS solution (adjusted to pH = 7.4) containing one of the six peptides in 0.8 mM; for the K_{cp} measurements, the buffer solutions additionally contained PEG 8000 in various mass ratios to apply varied osmotic stresses to the lipid supramolecular structures [23]. The lipid dispersions were then subjected to vigorous vortex, cycling between two microsyringes (Avanti) without the extrusion orifice for 100 times, and freeze-thaw cycles more than 10 times to ensure sample homogeneity. The sample containers were filled with argon gas, sealed with parafilm, and stored at 4 °C for further homogenization before being used within 2 days. Each sample had a fixed lipid composition, fixed peptide identity and concentration, and, in the case of the K_{cp} measurements, fixed mass ratio for PEG 8000. All the prepared samples are listed in Table I.

C. C_0 and K_{cp} measurements

C_0 was determined with x-ray diffraction. The measurements were conducted at Beamlines BL13A1 and BL23A1 of the National Synchrotron Radiation Research Center (NSRRC) in Hsinchu, Taiwan, using x-rays of 12 and 15 keV, respectively. Prior to the data collection, the samples were inspected for their homogeneity by comparing the x-ray diffraction images taken from different parts of a sample; any significant discrepancy in diffraction pattern (i.e., peak positions and relative intensities), which are signs of sample inhomogeneity, would exclude a sample from the data collection. The x-ray diffraction data from the qualified samples were collected at 25 °C with a Mar 165 CCD detector at BL13A1 and a Pilatus 1MF pixel detector at BL23A1. The raw diffraction images collected at BL13A1 and BL23A1 were azimuthally integrated and background-subtracted with the program TVX (version 7.2, courtesy of Prof. Sol Gruner and Dr. Mark Tate of Cornell University) and the in-house program provided at BL23A1, respectively; x-ray absorption was taken into consideration for the background subtraction. The reduced data were expressed as one-dimensional (1D) diffraction profiles where the diffraction intensity was plotted against $|\vec{Q}| = 4\pi \sin\theta/\lambda$, with λ and θ being the x-ray wavelength and half of the diffraction angle, respectively [Fig. 1(a)].

The reduced data were used to reconstruct the electron density profiles following the procedure depicted in Ref. [16]. Briefly, the diffraction peaks were fitted with the Voigt functions to extract peak intensities I_q's (i.e., the area under peak) [Fig. 1(a)]. Subsequently, via $A_q^2 \propto I_q \sin\theta/m$, where m is the multiplicity factor, I_q's were related to the Fourier coefficients A_q's in the Fourier series of cosines, which expressed the electron density distribution $\rho_e(\vec{r})$ within a centrosymmetric unit cell. With $\rho_e(\vec{r})$ expressed as $\rho_e(\vec{r}) = \sum_q A_q \cos(\vec{Q}\cdot\vec{r})$, we could reconstruct the electron density profiles for given samples, provided the signs of the A_q's (i.e., the phase of the

TABLE I. Samples conditions examined in this study. Three or more samples were prepared for most of the conditions.

peptide species / PEG 8000 concentration (wt%)	None	K6	K9	$(K2W)^2$	K4W2	R6	R9
Pure DOPE monolayers in the H_{II} phase							
0	Δ	Δ	Δ	Δ	Δ	Δ	Δ
4.0	Δ	Δ	Δ	Δ	Δ	Δ	
6.4	Δ	Δ	Δ	Δ		Δ	
8.3	Δ	Δ	Δ	Δ	Δ	Δ	
10.7	Δ	Δ	Δ	Δ	Δ		Δ
14.7	Δ	Δ	Δ	Δ	Δ	Δ	Δ
17.9	Δ	Δ	Δ	Δ	Δ		Δ
21.7	Δ	Δ	Δ	Δ	Δ	Δ	Δ
DOPE+DOPA monolayers in the H_{II} phase							
0	Δ	Δ	Δ	Δ	Δ		
4.0	Δ	Δ	Δ	Δ	Δ		
6.4	Δ	Δ	Δ	Δ	Δ		
8.3	Δ	Δ	Δ	Δ	Δ		
10.7	Δ	Δ	Δ	Δ	Δ		
14.7	Δ	Δ	Δ	Δ	Δ		
17.9	Δ	Δ		Δ	Δ		
21.7	Δ	Δ	Δ	Δ	Δ		

diffracted electromagnetic waves) had been known when the I_q's were converted to A_q's (see below). Once the electron density profile is reconstructed, the structural information of lipid supramolecular structures is readily extractable because of the high electron density contrast between the hydrophilic head and hydrophobic hydrocarbon (HC) chains of a lipid molecule. The information can then be used to determine C_0, as described below.

Owing to the overwhelming dominance of DOPE in the compositions, the lipids favored the inverted hexagonal H_{II} phase. In this configuration, a lipid monolayer cylindrically wraps around water to form a cylindrical core-shell structure, with the core and shell being water and the HC chains, respectively, and with the lipid heads lying in between; the cylinders are in turn stacked upon one another into a two-dimensional (2D) hexagonal lattice with centrosymmetry. With the signs of the A_q's assigned as "+", "−", "−", "+", "+", "+", and "+" for the diffraction peaks with Miller indices of (1,0), (1,1), (2,0), (2,1), (3,0), (2,2), and (3,1), respectively, we employed the procedure described above to reconstruct the electron density profiles for the lipid monolayers in the H_{II} phase [Fig. 1(b)]. (The phasing was assigned as suggested in Ref. [16], given that the lipid composition adopted here was identical to that in the literature and the peptides exerted only decent effects on the monolayer structure. Visual inspections of the other phasing options supported the adoption of the current phasing.) From the reconstructed 2D electron density profiles, the radius of the water core R_w was determined from the positions of the electron-dense heads and subsequently converted to the distance R_p between the cylindrical axis and the pivotal plane, a dividing plane within a lipid monolayer where the cross-sectional area of a lipid molecule remains unchanged upon isothermal bending. Generally, R_p is not directly related to C_0 because the intersecting region among any three neighboring cylinders requires the HC chains to extend differentially or the lipid-water interface distorts from an ideal circular shape to fill; both of the two configurational requirements, collectively known as packing frustration, are energetically costly and thus energetically contribute to the determination of the conformations favored by a lipid monolayer. Since present only in the inverted nonplanar lipid phases (e.g., the H_{II} phase), the packing frustration favors planar monolayer conformations over the inverted nonplanar conformations. The addition of free long hydrocarbons, such as tetradecane, can relieve the packing frustration, presumably due to their preferential partition to the intersection regions [24]. In the absence of packing frustration, the conformation assumed by a lipid monolayer is dictated by its C_0, and R_p determined in this condition is the equivalent of the spontaneous radius of curvature $R_{0p} = 1/C_0$ [16,17].

K_{cp} was determined similarly. The PEG 8000 molecules in the samples (with or without the peptides) for the K_{cp} measurements applied osmotic stresses Π's to the lipid-water cylinders, since the size of the molecules, with Flory radius of ∼8 nm, restricted them from entering the water cores of the cylinders (<4 nm in diameter) and thus provided water the driving force to leave the water cores. This effectively bent a lipid monolayer and shrank R_p to the extent depending on the K_{cp} of the lipid monolayer. Once the electron density profiles were reconstructed for a series of *independent* samples with identical lipid and peptide compositions but varied Π's, the relation of R_p as a function of Π could be established. Through fitting the equation [25]

$$\Pi R_p^2 = 2K_{cp}(1/R_p - 1/R_{0p}) \tag{1}$$

against the data, we determined the K_{cp}'s for the samples of different lipid and peptide compositions.

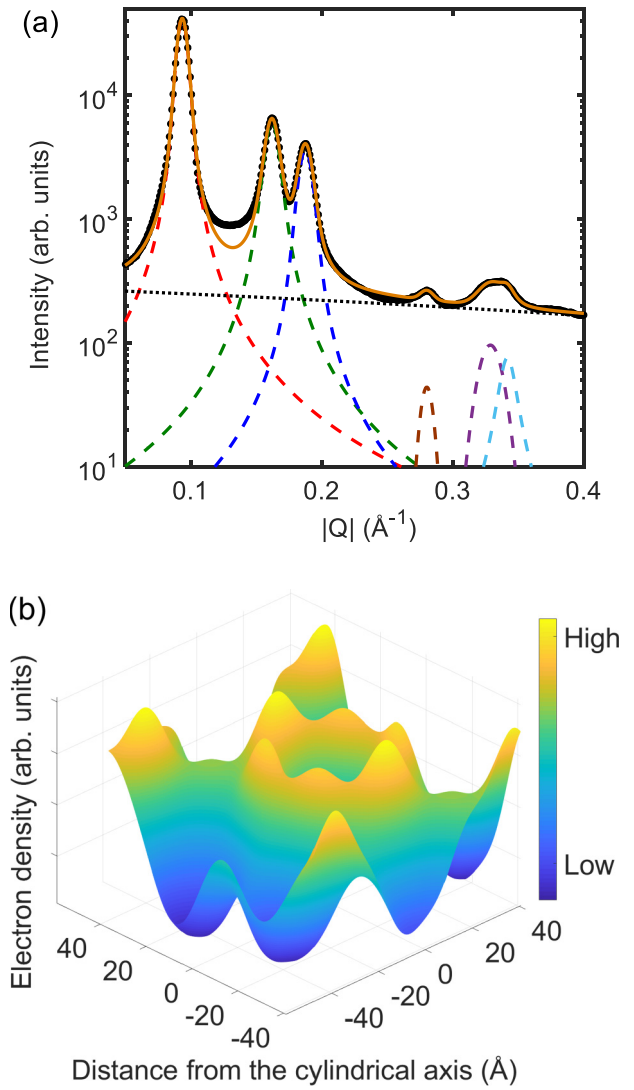

FIG. 1. 1D diffraction profile (a) and 2D electron density profile (b) for the DOPE monolayers with the configuration of the H_{II} phase. In (a), the monolayers were incubated with $(K2W)^2$, while no peptide was present for (b). Each peak in (a) was fitted with the Voigt function (dashed lines) on top of a linear background (black dotted line); the sum of the fitting functions is lineated with the orange solid line, which fits well with the data (filled circles). Within the region surrounded by the electron density peaks in (b) is the water core of the H_{II} phase.

III. RESULTS

A. The dependence of K_{cp} on the monolayer-peptide interaction

The variation in the K_{cp}'s of the DOPE and DOPE+DOPA monolayers with the configuration of the H_{II} phase was examined to understand how K_{cp} had reacted to the presence of the peptides mimicking the microbicidal-potent AMP mutants [i.e., $(K2W)^2$, K4W2, R6, and R9] and their impotent counterparts (i.e., K6 and K9) in Wong and colleagues' studies [13]. Figure 2 shows the $\Pi R_p^2 - 1/R_p$ correlations from the DOPE and DOPE+DOPA monolayers in the different Π's effected by PEG 8000 of different concentrations (refer to Table I for the concentrations of PEG 8000) in the presence or absence of the peptides; with Eq. (1), K_{cp} can be extracted from these correlations. Since the slope of a linear fitting to the correlation gives K_{cp}, one can assess how extensively K_{cp} was varied by the peptides via examining the slope change relative to the peptide-free case. When the monolayers were solely composed of DOPE, incubating the monolayers with K6 resulted in a slope, 11.9 [Fig. 2(b)], essentially identical to that of the peptide-free monolayers, 12.5 [Fig. 2(a)], whereas slope variations are clearly seen for some other peptides, e.g., $(K2W)^2$ and R6 being 16.5 and 19.0, respectively [Figs. 2(c) and 2(d)]. On the contrary, with the incorporation of only 4 mol % anionic DOPA, the monolayers exhibited considerable changes in slope when incubated with any of the peptides, e.g., from 10.5 for the peptide-free case to 20.0 for the case of K6 [Figs. 2(f)–2(h)].

The fairly good linearity displayed by the $\Pi R_p^2 - 1/R_p$ correlations has allowed us to determine K_{cp} with decent confidence (Fig. 3). As observed in Fig. 2, the extent of the K_{cp} variation strongly depended on the identity of the peptide added when monolayers were purely made of DOPE. K6, belonging to the impotent category, had essentially no effect on the K_{cp} of the DOPE monolayers, whereas its elongated cousin in the same category, K9, compromised the monolayers' rigidity, albeit only marginally. Incorporating W (the HAA used here) to the Ks greatly enhanced a K peptide's influence on K_{cp}. $(K2W)^2$ and K4W2, both categorized to the potent group, increased the monolayers' rigidity, with the difference in sequence between the two peptides resulting in different extents of stiffening. This discrepancy in effect on K_{cp} between K6 and K9 against $(K2W)^2$ and K4W2 may arise from the difference in their interactions with the monolayers; the Ws in the latter likely strengthened the monolayer-peptide interaction and drove the peptides' insertion into the monolayers via the hydrophobic effect. In this context, it is remarkable to see that, even without W, R6 and R9, the other peptides in the potent category, could still perturb K_{cp} substantially, with strengths comparable to those for $(K2W)^2$ and K4W2.

Consistent with the observation in Fig. 2, incorporating a trace of DOPA into the DOPE monolayers enabled all the peptides to generate significant and comparable effects on K_{cp}. The electrostatic interaction afforded by the cationic AAs and anionic DOPA may enhance the monolayer-peptide interaction and thus the peptides' effect on K_{cp}. All the K_{cp} data are compiled in Table II. (Note: The uncertainties for the K_{cp}'s were determined following the standard statistical method for estimating the uncertainty intrinsic to a linear fitting. Their values depended on factors such as the number of data points and fitting quality and were not explicitly related to the uncertainties associated with the R_p measurements, which were mostly smaller than the symbols in Fig. 2.)

A comparison of the data in the literature where K_{cp} was either obtained from the monolayers in the H_{II} phase employing the same method as adopted here (e.g., $K_{cp} = 0.40 \times 10^{-19}$ J for DOPC [23]) or from the monolayers in a planar conformation using the micropipette-aspiration technique (e.g., $K_{cp} = 0.42 \times 10^{-19}$ J for DOPC [26]) reveals good agreement between the data determined with the two means and the two monolayer conformations. This eases the concern over the applicability to planar monolayers of insights

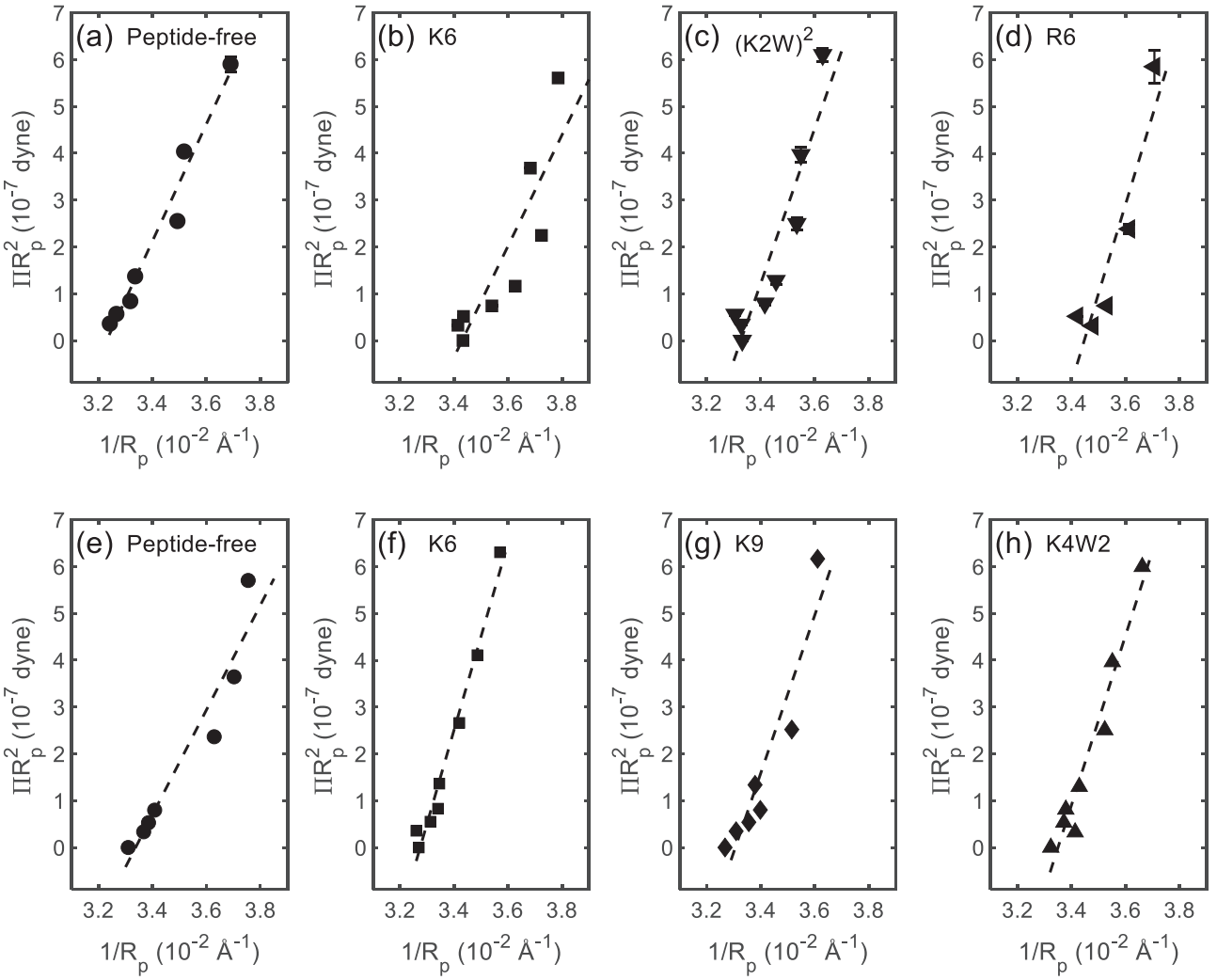

FIG. 2. Correlation between the applied osmotic stress Π and the structural dimension R_p of the H_{II} structure formed by the DOPE (a–d) and DOPE+DOPA (molar ration = 96 : 4), (e–h) monolayers in the absence or presence of the peptides. The slopes reflect the K_{cp}'s [see Eq. (1)]. For most cases, uncertainty is smaller than the symbols.

learned from examining the elastic properties determined with the monolayers in the H_{II} phase.

B. The peptides' lack of influence on C_0

The peptides' influences on C_0 were also scrutinized (Fig. 4 and Table II). Surprisingly, for both the DOPE and DOPE+DOPA monolayers, all the peptides had no effect on C_0, whether they belonged to the microbicidal-potent or impotent categories; even with the supposed presence of the electrostatic interaction, the peptides remained incapable of perturbing the C_0 of the monolayers (Fig. 4). One may suspect that the insensitivity of C_0 to the peptides indicates the absence of the monolayer-peptide interaction. For certain combinations of peptide species and lipid composition (i.e., K6 and pure DOPE), this speculation may be warranted. Nevertheless, given the strong variation in K_{cp} in the other cases (Fig. 3), interaction had more than likely occurred between the peptides and lipid monolayers.

However, one may cite a concern over artificial effects arising from the application of osmotic stress to dispute this conclusion. The potential artifacts, one may argue, change the binding, insertion, or partitioning of the peptides to the monolayers and thus cast doubts on the validity or fidelity of the results of our K_{cp} measurements. To see whether the application of osmotic stress had any substantial effect on our measurements, we rearranged our K_{cp} data into figures similar to those in Fig. 2 but with the part of the data collected from the PEG-free samples excluded. The $\Pi R_p^2 - 1/R_p$ correlations thereby obtained were then used to determine the y intercepts of the linear fits, which, according to Eq. (1), are $-2K_{cp}/R_{0p}$ and thus give values of C_0. Were the osmotic stress influential to the aspects of the monolayer-peptide interaction concerned here, one would see discrepancies between the C_0's determined exclusively with the PEG-containing samples and the C_0's presented in the main panel of Fig. 4, which were derived directly from the electron density profiles of the PEG-free samples. Remarkably, the C_0's determined with the two methods and sample groups are in excellent agreement with one another (inset of Fig. 4), thus vindicating the osmotic-stress-mediated method and the data it accrued.

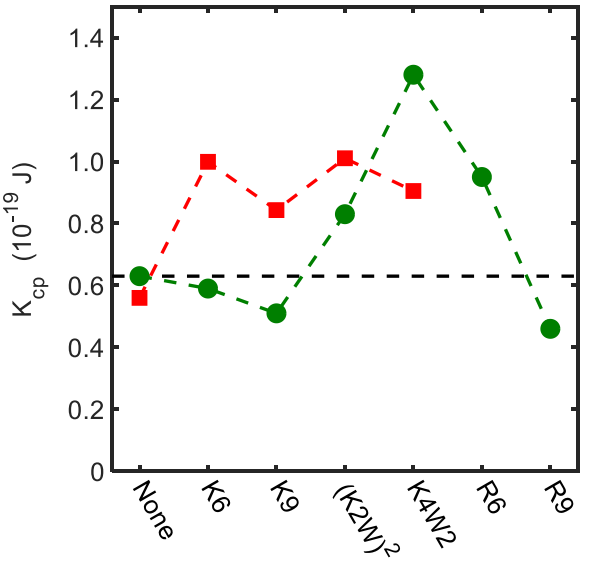

FIG. 3. Bending modulus K_{cp} for the DOPE (green filled circles) and DOPE+DOPA (molar ration = 96 : 4) (red filled squares) monolayers in the absence or presence of the investigated peptides.

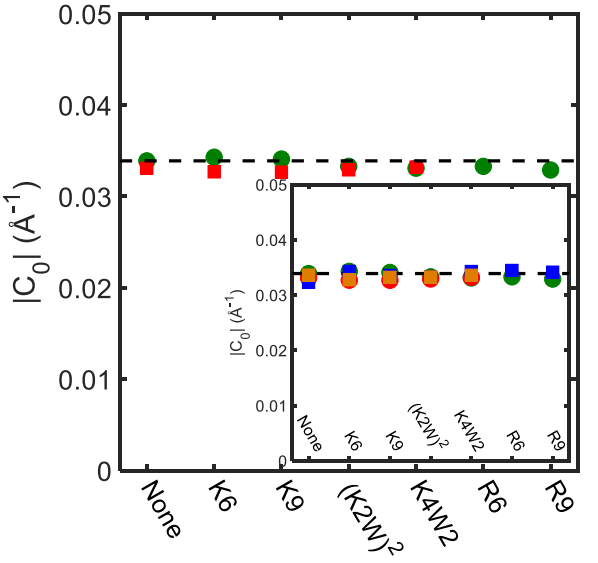

FIG. 4. Spontaneous curvature C_0 for the DOPE (green filled circles) and DOPE+DOPA (molar ration = 96 : 4) (red filled squares) monolayers in the absence or presence of the investigated peptides. Inset compares the C_0's extracted from the PEG-free samples (green and red filled circles) with those exclusively from the PEG-containing samples (blue and amber filled squares).

IV. DISCUSSION

A. The peptides' insertion into the monolayers and perturbation in the molecular packing

The observation that the potency-categorized peptides were able to modulate the K_{cp}'s of the DOPE monolayers but not their C_0's is quite puzzling. Since peptides' influences on K_{cp} and C_0 are exerted through their insertion into lipid monolayers and their perturbation in the molecular packing of lipid [27–31], we examined the reconstructed electron density profiles, attempting to look into the insertion depth of the peptides and their perturbation in the molecular packing of the DOPE monolayers with the H_{II} configuration. The 1D electron density profiles shown in Fig. 5, obtained by azimuthally averaging the 2D electron density profiles and scaled to the electron densities of water in the cylindrical core and the methyl termini of DOPE ($\rho_e = 0.334\,e^-/Å^{-3}$ and $\rho_e = 0.22\,e^-/Å^{-3}$, respectively), present the electron densities along the radial distance from the cylindrical axis of the H_{II} phase. The DOPE monolayers in the absence of any peptide and in the presence of K6 display a depression in electron density right before the peak marking the location of the phosphate group; the depression is also observed in the literature for DOPE in the H_{II} phase [17]. This depression is absent for the monolayers incubated with $(K2W)^2$. Moreover, compared to the monolayers alone and with K6, incubating the monolayers with the potency-categorized peptide also resulted in an electron density elevation at the peak and the positions further into the monolayers (Fig. 5). It can be inferred from the observations that the potency-categorized $(K2W)^2$ could perturb the molecular packing from the phosphate group down to the HC chain termini, while the impotency-categorized K6 could not. Also, as an electron density elevation in the HC chain region implies an increase in the packing density of the HC chains and thus in the packing order, the stiffening effect

TABLE II. The C_0's and K_{cp}'s determined in this study. The uncertainty for K_{cp} is intrinsic to the linear fitting used to determine the K_{cp}'s and not from the measurement uncertainty for the data points in the fitting.

Peptide species \ Monolayer elastic properties	C_0 (Å^{-1})	K_{cp} (10^{-19} J)	C_0 (Å^{-1})	K_{cp} (10^{-19} J)
	Pure DOPE monolayers in the H_{II} phase		DOPE + DOPA monolayers in the H_{II} phase	
None	-0.0339 ± 0.0005	0.63 ± 0.11	-0.0331 ± 0.0005	0.56 ± 0.19
K6	-0.0343 ± 0.0006	0.59 ± 0.26	-0.0327 ± 0.0001	1.00 ± 0.13
K9	-0.0341 ± 0.0002	0.51 ± 0.24	-0.0327 ± 0.0001	0.84 ± 0.28
$(K2W)^2$	-0.0333 ± 0.0002	0.83 ± 0.26	-0.0329 ± 0.0001	1.01 ± 0.32
K4W2	-0.0331 ± 0.0003	1.28 ± 0.56	-0.0332 ± 0.0002	0.90 ± 0.17
R6	-0.0333 ± 0.0003	0.95 ± 0.54	-	-
R9	-0.0329 ± 0.0002	0.46 ± 0.28	-	-

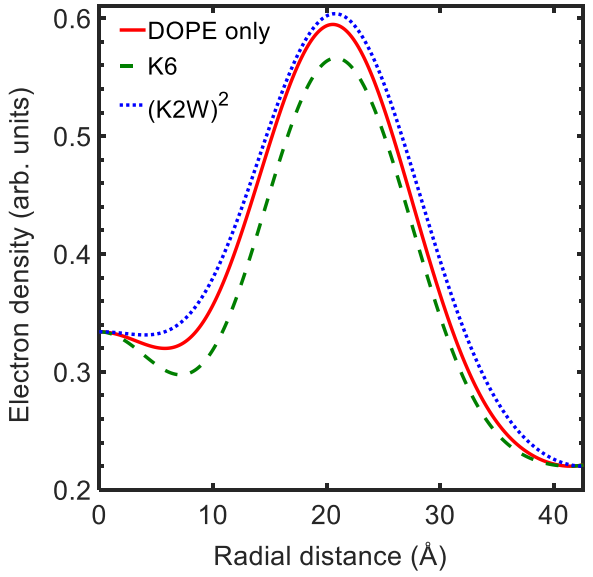

FIG. 5. 1D electron density profiles for the DOPE monolayers alone (solid line) or incubated with K6 (dashed line) or $(K2W)^2$ (dotted line). The origin of the abscissa marks the position of the cylindrical axis in the H_{II} phase. The peak arose from the electron-dense phosphate group in the head of DOPE.

on the DOPE monolayers of $(K2W)^2$ (Fig. 3) is ascribable to the ordering effect of its perturbation. This is consistent with a very recent x-ray scattering and neutron reflectivity study where the AMP, colistin, was shown to increase the packing order of the HC chains and thereby stiffen a lipid model membrane mimicking the biomembranes of Gram-negative bacteria [21]. The ability to perturb the HC chains may be a general feature among the potency-categorized peptides studied here.

However, we refrain from pinpointing the exact position of $(K2W)^2$ inside the monolayers because of the limit on the resolution of the electron density profiles; while the radii of gyration for the short, random-coiled peptides were of the order of several angstroms, the best of our samples diffracted only to $\sim 0.36\,\text{Å}^{-1}$, corresponding to the finest resolvable length scale of tens of angstroms. Even so, some information regarding the potency-categorized peptides' insertion depth can still be gleaned from consulting the literature. It is known from the literature that, with a peptide's molecular axis parallel to the surface, shallow or deep peptide penetration makes C_0 more positive or negative, respectively, whereas inserting a peptide to an intermediate depth only minimally perturbs C_0 [32]. It is thus tempting to speculate that the peptides might have penetrated the monolayers to an intermediate depth and consequently left C_0 unperturbed.

B. The AMPs might induce transmembrane toroidal pores or membrane micellation by elevating or depressing K_{cp}

Membrane perforation by the AMPs often requires the planar monolayers constituting the membranes to undergo structural transformations into a nonplanar conformation and thus concerns the monolayers' elastic properties. The transformations face an energetic barrier equivalent of the elastic energy difference ΔG_E between the two conformations [33],

$$\begin{aligned}\Delta G_E &= \left[\frac{1}{2}K_{cp}\int_A (C-C_0)^2 dA + K_G\int_A G dA\right] \\ &\quad -\left[\frac{1}{2}K_{cp}\int_A C_0^2 dA\right] \\ &= K_{cp}\int_A\left(\frac{C^2}{2}-CC_0\right)dA + K_G\int_A G dA \\ &= K_{cp}\left(\frac{\langle C^2\rangle}{2}-\langle C\rangle C_0\right)A + K_G\langle G\rangle A, \end{aligned} \tag{2}$$

where the first and second brackets in the first equality represent the elastic energies of a nonplanar and planar conformations, respectively; C and G are the total and Gaussian curvatures of a monolayer, respectively; and $\langle\ldots\rangle$ denotes the average over surface area A. Note that C and G are the geometrical features of a given conformation; e.g., a planar conformation is featured with a zero C and G, while C and G are twice the reciprocal radius and reciprocal squared radius, respectively, when the conformation is spherical. On the other hand, K_{cp} and C_0 are elastic properties of a monolayer with a given composition and presumably *unchanged* upon structural transformations of the monolayer [23,34]. Therefore, insights learned here regarding the AMP mimics' influences on C_0 and K_{cp} are applicable to planar monolayers, even though this study was conducted on the monolayers with the configuration of the H_{II} phase.

Carpet and toroidal pore models are two models often invoked to account for the planar-to-nonplanar transformations of monolayers entailed by the AMP-mediated membrane perforation [35–37]. The toroidal pore model describes a transmembrane pore where the pore-lining AMPs mingle with the proximal lipid molecules and organize the lipid monolayers into a nonplanar conformation (Fig. 6). The surface of a toroidal pore bends toward the hydrophobic or hydrophilic part of the monolayer when the pore is side-viewed or top-viewed, respectively; that is, the surface has both positive and negative principal curvatures in two perpendicular directions [18]. This geometrical feature defines a negative G and a nonzero C, provided the pore radius differs from the monolayer thickness. To energetically favor the toroidal perforation,

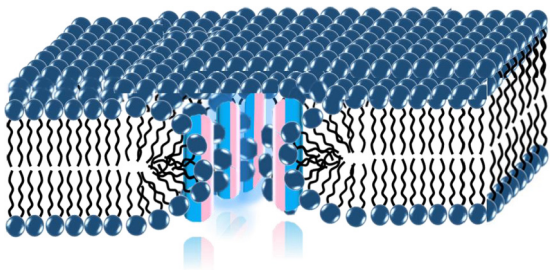

FIG. 6. Schematic illustration of a toroidal pore. Peptides are represented by the rodlike structures, with the hydrophobic part in light blue (dark gray) and hydrophilic part in pink (light gray).

which involves a nonplanar conformation with a negative G and nonzero C, ΔG_E in Eq. (2) must be negative; in other words, the following condition must be satisfied:

$$\frac{C_0\langle C\rangle}{\langle G\rangle} - \frac{\langle C^2\rangle}{2\langle G\rangle} < \frac{K_G}{K_{cp}}. \tag{3}$$

Accordingly, the AMPs must modulate the K_{cp}, C_0, or K_G of a monolayer to induce a toroidal pore having a specific $\langle C\rangle$ and $\langle G\rangle$. Obviously, the larger the K_G/K_{cp}, the better the chance of forming a toroidal pore. Given the considerable influences on K_{cp} and lack of influence on C_0 for all the potency-categorized peptides [i.e., $(K2W)^2$, K4W2, R6, and R9] (Figs. 3 and 4), one may infer that the energetic favorability of a toroidal pore having a specific $\langle C\rangle$ and $\langle G\rangle$ should depend on how extensively the Rs, Ks, or Ks coupled with HAAs in the AMPs modulate the K_G/K_{cp} of a monolayer. Given K_G being negative for lipid monolayers [38], one can even speculate that the AMPs capable of elevating K_{cp} facilitate the formation of a toroidal pore whereas the ones depressing K_{cp} suppress it.

On the other hand, the carpet model features membrane micellation, which involves the AMP-mediated extraction of the molecules from membranes and results in massive openings on them. The spherical shape of a micelle defines $\langle C\rangle$, $\langle C^2\rangle$, and G to be $2/r$, $4/r^2$, and $1/r^2$, respectively, with r being the micellar radius. Equation (2) is thus simplified to $\Delta G_E = 8\pi K_{cp}(1 - rC_0) + 4\pi K_G$ for membrane micellation. Since r reflects the length of the molecules in the monolayer, the energetic favorability of micellation is dictated by K_{cp}, C_0, and K_G. Again, based on Figs. 3 and 4, the Rs, Ks, or Ks coupled with HAAs in the AMPs are speculated to apply the microbicidal effect by modulating the K_{cp} and K_G of a monolayer. Interestingly, the micellation equivalence of Eq. (3), $2(rC_0 - 1) > K_G/K_{cp}$, appears to imply that the AMPs capable of softening membranes and thus hindering the formation of a toroidal pore may instead promote membrane micellation.

V. CONCLUSION

In their seminal works on defensin and the mutants, Wong and colleagues suggest that defensin and the potent mutants' capability of inducing transmembrane pores is ascribable to the interaction between pathogenic membranes and the Rs or the Ks coupled with HAAs in the AMPs, which facilitates formation of the nonplanar monolayer conformations featured with negative G's; on the other hand, the loss of the microbicidal capability from the K-for-R mutation is owing to the Ks' inability to promote the formation of such structures [9,13–15]. From the perspective of continuum mechanics, we have further dug into this understanding and investigated how the AMP mimics made of R, K, or K coupled with a HAA modulated the elastic properties of the lipid monolayers made of the dominant lipid in bacteria, and thereby quantified the qualitative description of Wong and colleagues. Based on the experimental evidence and energetic analyses presented above, we argue that how readily the monolayer of a pathogenic membrane can assume the nonplanar conformations, including those featured with negative G's, leading to the pathogen's death under an AMP's act, strongly depends on how extensively the AMP can modulate the K_{cp} of the monolayer. Indeed, that the impotency-categorized K6 and K9 were unable to modulate the K_{cp} of DOPE monolayers while the potency-categorized $(K2W)^2$, K4W2, R6, and R9 could is consistent with and accounts for Wong and colleagues' observations. It is further inferred here that what mechanism (toroidal pores or membrane micellation) is followed by an AMP in killing a pathogen hinges, at least partially, on how the AMP alters the K_{cp} of the pathogenic monolayer, with stiffening and softening leading to toroidal pores and membrane micellation, respectively. Therefore examining a synthetic peptide's influence on K_{cp} may reveal its efficacy as an AMP and even its mode of action, thus constituting an efficient screening tool and design principle for developing synthetic AMPs. This point is supported by a recent study where colistin's ability to kill Gram-negative but not Gram-positive bacteria was related to its ability to perturb the K_{cp}'s of the former [21].

The observation that C_0 was irresponsive to the presence of our AMP mimics, whether the lipid monolayers were made of zwitterionic DOPE only or its mixture with anionic DOPA, is surprising. A rich trove of published data claim to have observed the perturbation in the C_0's of diverse lipid membrane systems by a variety of membrane-active peptides, including AMPs (Ref. [19] and references therein). Nevertheless, most of these data are regarding the peptide-induced variations in the planar-to-nonplanar phase transition temperatures; none of them, to the best of our knowledge, involves direct measurements on C_0. As manifested in Eq. (2), the energetic favorability and thus the transition temperature for a nonplanar phase, are not only dictated by C_0 but also other elastic properties. Based on our direct measurements on the C_0's and K_{cp}'s of the monolayers incubated with the AMP mimics, we raise the possibility that the AMP-induced variations in the planar-to-nonplanar phase transition temperatures might have mainly arisen from the variation in K_{cp} and also likely from the variation in K_G, rather than from the variation in C_0. This reassessment of how significant the C_0 variation is to the structural transformations of membranes resonates well with recent studies on membrane fusion [23,33], another cellular activity involving planar-to-nonplanar transformations. In Ref. [23], C_0 was concluded to have less fusogenical importance than conventionally presumed, whereas the long overlooked K_{cp} was found to be a fusogenically potent factor. The two reevaluations of C_0 might hint at a new paradigm general to the cellular events involving nonplanar monolayer conformations. Based on the recently confirmed relation between membrane elasticity and dynamics [30], this new paradigm, if at all, might even have a dynamical flavor.

ACKNOWLEDGMENTS

This paper was supported by the Ministry of Science and Technology (Grant No. MOST 106-2628-E-008-003-MY3) and by National Central University.

W.-F.C. and S.-H.C. contributed equally to this work.

[1] M. Mahlapuu, J. Håkansson, L. Ringstad, and C. Björn, Front. Cell Infect. Microbiol. **6**, 194 (2016).
[2] S. Cociancich, A. Ghazi, C. Hetru, J. A. Hoffmann, and L. Letellier, J. Biol. Chem. **268**, 19239 (1993).
[3] K. Matsuzaki, K. Sugishita, M. Harada, N. Fujii, and K. Miyajima, Biochim. Biophys. Acta **1327**, 119 (1997).
[4] H. Yao, M. W. Lee, A. J. Waring, G. C. Wong, and M. Hong, Proc. Natl. Acad. Sci. USA **112**, 10926 (2015).
[5] F. Sgolastra, B. M. Deronde, J. M. Sarapas, A. Som, and G. N. Tew, Acc. Chem. Res. **46**, 2977 (2013).
[6] C. L. Bergstrom, P. A. Beales, Y. Lv, T. K. Vanderlick, and J. T. Groves, Proc. Natl. Acad. Sci. USA **110**, 6269 (2013).
[7] M. Fuhrmans and S. J. Marrink, J. Am. Chem. Soc. **134**, 1543 (2012).
[8] E. Y. Lee, B. M. Fulan, G. C. Wong, and A. L. Ferguson, Proc. Natl. Acad. Sci. USA **113**, 13588 (2016).
[9] N. W. Schmidt and G. C. Wong, Curr. Opin. Solid State Mater. Sci. **17**, 151 (2013).
[10] J. S. Bahnsen, H. Franzyk, A. Sandberg-Schaal, and H. M. Nielsen, Biochim. Biophys. Acta **1828**, 223 (2013).
[11] I. Schiopu, L. Mereuta, A. Apetrei, Y. Park, K. S. Hahm, and T. Luchian, Mol. Biosyst. **8**, 2860 (2012).
[12] P. Nicolas and A. Mor, Annu. Rev. Microbiol. **49**, 277 (1995).
[13] N. W. Schmidt, K. P. Tai, K. Kamdar, A. Mishra, G. H. Lai, K. Zhao, A. J. Ouellette, and G. C. Wong, J. Biol. Chem. **287**, 21866 (2012).
[14] N. W. Schmidt, M. Lis, K. Zhao, G. H. Lai, A. N. Alexandrova, G. N. Tew, and G. C. Wong, J. Am. Chem. Soc. **134**, 19207 (2012).
[15] N. W. Schmidt, A. Mishra, G. H. Lai, M. Davis, L. K. Sanders, D. Tran, A. Garcia, K. P. Tai, P. B. McCray, A. J. Ouellette, M. E. Selsted, and G. C. Wong, J. Am. Chem. Soc. **133**, 6720 (2011).
[16] Y.-F. Chen, K.-Y. Tsang, W.-F. Chang, and Z.-A. Fan, Soft Matter **11**, 4041 (2015).
[17] B. Kollmitzer, P. Heftberger, M. Rappolt, and G. Pabst, Soft Matter **9**, 10877 (2013).
[18] G. C. Shearman, O. Ces, R. H. Templer, and J. M. Seddon, J. Phys.: Condens. Matter **18**, S1105 (2006).
[19] D. Koller and K. Lohner, Biochim. Biophys. Acta **1838**, 2250 (2014).
[20] J. H. Lee, S. M. Choi, C. Doe, A. Faraone, P. A. Pincus, and S. R. Kline, Phys. Rev. Lett. **105**, 038101 (2010).
[21] F. G. Dupuy, I. Pagano, K. Andenoro, M. F. Peralta, Y. Elhady, F. Heinrich, and S. Tristram-Nagle, Biophys. J. **114**, 919 (2018).
[22] R. M. Epand and R. F. Epand, Biochim. Biophys. Acta **1788**, 289 (2009).
[23] Z.-A. Fan, K.-Y. Tsang, S.-H. Chen, and Y.-F. Chen, Sci. Rep. **6**, 31470 (2016).
[24] S. M. Gruner, Proc. Natl. Acad. Sci. USA **82**, 3665 (1985).
[25] N. Fuller, C. R. Benatti, and R. P. Rand, Biophys. J. **85**, 1667 (2003).
[26] W. Rawicz, K. C. Olbrich, T. McIntosh, D. Needham, and E. Evans, Biophys. J. **79**, 328 (2000).
[27] R. M. Epand, K. D'Souza, B. Berno, and M. Schlame, Biochim. Biophys. Acta **1848**, 220 (2015).
[28] C. Galanth, F. Abbassi, O. Lequin, J. Ayala-Sanmartin, A. Ladram, P. Nicolas, and M. Amiche, Biochemistry **48**, 313 (2009).
[29] T. Doherty, A. J. Waring, and M. Hong, Biochim. Biophys. Acta **1758**, 1285 (2006).
[30] K.-Y. Tsang, Y.-C. Lai, Y.-W. Chiang, and Y.-F. Chen, Phys. Rev. E **96**, 012410 (2017).
[31] B. Kollmitzer, P. Heftberger, R. Podgornik, J. F. Nagle, and G. Pabst, Biophys. J. **108**, 2833 (2015).
[32] A. Zemel, A. Ben-Shaul, and S. May, J. Phys. Chem. B **112**, 6988 (2008).
[33] S. Aeffner, T. Reusch, B. Weinhausen, and T. Salditt, Proc. Natl. Acad. Sci. USA **109**, E1609 (2012).
[34] R. M. Venable, F. L. H. Brown, and R. W. Pastor, Chem. Phys. Lipids **192**, 60 (2015).
[35] M. A. Sani and F. Separovic, Acc. Chem. Res. **49**, 1130 (2016).
[36] W. C. Wimley, ACS Chem. Biol. **5**, 905 (2010).
[37] K. A. Brogden, Nat. Rev. Microbiol. **3**, 238 (2005).
[38] D. P. Siegel and M. M. Kozlov, Biophys. J. **87**, 366 (2004).